

Tri-band high temperature superconducting filter with a wide stopband designed using a step impedance hairpin ring resonator

Zhaojiang Shang(商兆江), Weijin Yang(杨伟进), Yan Zhang(张艳), and Liguo Zhou(周立国)
Citation: Chin. Phys. B, 2026, 35 (**6**): 068501. DOI: 10.1088/1674-1056/ae13eb
http://cpb.iphy.ac.cn; http://iopscience.iop.org/cpb

What follows is a list of articles you may be interested in

Design of sextuple-mode triple-ring HTS UWB filter using two-round interpolation

Ming-En Tian(田明恩), Zhi-He Long(龙之河), You Lan(蓝友), Lei-Lei He(贺磊磊), and Tian-Liang Zhang(张天良)
Chin. Phys. B, 2021, 30 (**5**): 058503. DOI: 10.1088/1674-1056/abd7e1

Compact high-order quint-band superconducting band-pass filter

Di Wu(吴荻), Bin Wei(魏斌), Xi-Long Lu(陆喜龙), Xin-Xiang Lu(卢新祥), Xu-Bo Guo(郭旭波), Bi-Song Cao(曹必松)
Chin. Phys. B, 2018, 27 (**6**): 068503. DOI: 10.1088/1674-1056/27/6/068503

Compact wide stopband superconducting bandpass filter using modified spiral resonators with interdigital structure

Di Wu(吴荻), Bin Wei(魏斌), Bo Li(李博), Xu-Bo Guo(郭旭波), Xin-Xiang Lu(卢新祥), Bi-Song Cao(曹必松)
Chin. Phys. B, 2018, 27 (**6**): 068502. DOI: 10.1088/1674-1056/27/6/068502

Compact superconducting single-and dual-band filter design using multimode stepped-impedance resonator

Xiang Wang(王翔), Bin Wei(魏斌), Xi-Long Lu(陆喜龙), Xu-Bo Guo(郭旭波), Bi-Song Cao(曹必松)
Chin. Phys. B, 2017, 26 (**12**): 128501. DOI: 10.1088/1674-1056/26/12/128501

A high-temperature superconducting filter withcontrollable transmission zero

Tianqi Gao(高天琪), Bin Wei(魏斌), Yong Heng(衡勇)
Chin. Phys. B, 2017, 26 (**5**): 058503. DOI: 10.1088/1674-1056/26/5/058503

Tri-band high temperature superconducting filter with a wide stopband designed using a step impedance hairpin ring resonator

Zhaojiang Shang(商兆江)[1], Weijin Yang(杨伟进)[1], Yan Zhang(张艳)[1], and Liguo Zhou(周立国)[2,†]

[1] *College of Science, Shanghai Institute of Technology, Shanghai* 201418, *China*
[2] *School of Health Science and Engineering, University of Shanghai for Science and Technology, Shanghai* 200093, *China*

(Received 4 June 2025; revised manuscript received 21 September 2025; accepted manuscript online 16 October 2025)

A high-temperature superconducting (HTS) tri-band bandpass filter with a step impedance hairpin ring resonator (SIHRR) was designed. The filter adopts the parallel mode of the loop resonator and the U-type step impedance resonator. The resonance mechanism of the resonator was studied, and the filter research process is described in detail. The three passbands can be independently adjusted by introducing an H-shaped secondary coupling structure. Finally, a third-order HTS filter with center frequencies and bandwidths of 3490 MHz (3.6%), 4290 MHz (3.4%), and 5190 MHz (5.1%) was successfully fabricated using photolithography and ion etching. The obtained filter had an out-of-band rejection of more than 37 dB up to 12 GHz, and the measurement results were in good agreement with the simulation results. Moreover, the structure of the filter is compact, with dimensions of 14 mm $\times$18 mm, which is equal to 0.53 $\lambda_g \times 0.3\lambda_g$.

Keywords: high-temperature superconducting, secondary coupling structure, SIHRR, tri-band bandpass filter
PACS: 85.25.–j
DOI: 10.1088/1674-1056/ae13eb **CSTR:** 32038.14.CPB.ae13eb

1. Introduction

In recent years, multifrequency bandpass filters have emerged as crucial components of modern wireless communication systems. Among these, triband passband filters have gained widespread application. Consequently, extensive research has been conducted on tri-band passband filters, leading to the proposal of numerous novel structures and design methodologies.[1–7] One approach involves splitting a single passband into three distinct passbands, as demonstrated in Ref. [1], where two open-circuit stubs are employed for this purpose. However, this method presents challenges when scaling to higher orders. To achieve high-order filtering capabilities, a tri-band filter can be realized by cascading two or three pairs of resonators.[2,3] Nevertheless, because of the inclusion of multiple filter types in their architecture, such designs often result in larger circuit sizes. To address the size constraints while maintaining performance efficiency, multimode resonators have been utilized in the design of compact tri-band filters.[4,9] Additionally, various innovative resonator configurations, including self-embedding asymmetric stepped impedance resonator (SE-ASIR),[10] coupled line step impedance resonators,[11] embedded microstrip-loaded resonators,[12] and zigzag line open-loop resonators,[13] have also proven effective for constructing tri-band filters with superior filtering characteristics. However, many existing triband filters exhibit diminished out-of-band rejection performance owing to the intensity of their first frequency doubling distance.

This paper presents a compact high-temperature superconducting filter designed using parallel configurations of hairpin ring and U-type step-impedance resonators. Through a theoretical analysis of the proposed resonator structure, we developed a controllable tri-band bandpass filter characterized by adjustable center frequencies and bandwidths achieved through variations in the coupling coefficients and impedance ratios. The central frequencies for our designed tri-band bandpass filter were 3500 MHz, 4300 MHz, and 5200 MHz; the corresponding bandwidths were measured at 3.6%, 3.4%, and 5.1%. This configuration demonstrates excellent stopband suppression characteristics while simultaneously generating multiple transmission zeros that enhance the passband selectivity.

2. Resonator analysis

Figure 1 shows the structural diagram of the proposed third-order bandpass high-temperature superconducting filter. In this design, a step-impedance hairpin ring resonator (SIHRR) was introduced in parallel with a half-wavelength bending step-impedance resonator. The half- and full-wavelength microstrip lines depicted in Fig. 2(a) were substi-

†Corresponding author. E-mail: zlg@usst.edu.cn
© 2026 Chinese Physical Society and IOP Publishing Ltd. All rights, including for text and data mining, AI training, and similar technologies, are reserved.

tuted by a transmitting half-wavelength step-impedance resonator (SIR) and a full-wavelength SIR, respectively. The resulting SIHRR configuration is shown in Fig. 2(b). Generally, SIRs are employed to design dual- or triple-band filters, whereas SIHRR serves to establish both the first and third passbands in this study. In addition, the first few resonant frequencies of a SIR can be adjusted by changing the impedance ratio and length of the resonator. By taking advantage of this feature, by altering the impedance ratio of the SIHRR, the parasitic frequency can be pushed up, thereby enabling the resonator to have excellent wide stopband performance. The SIHRR exhibits two operational modes: odd and even.

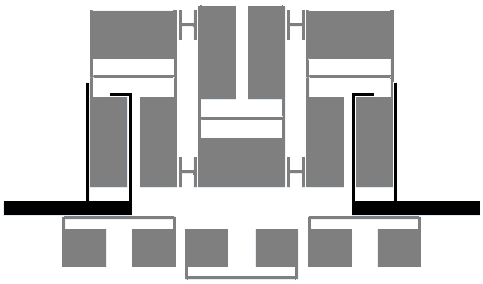


Fig. 1. Overall layout diagram of the third-order bandpass filter.

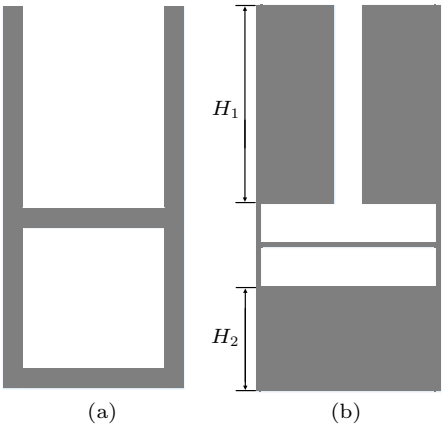


Fig. 2. Evolution of SIHRR: (a) traditional HRR, (b) proposed SIHRR.

Figure 3 shows the analog current density distribution of the SIHRR under parity-mode conditions. The findings indicate that at frequencies corresponding to the odd mode, the current predominantly concentrates on the two long open stub lines as well as on the horizontal line. Conversely, at the even-mode frequencies, the current concentration shifts primarily to the two long open stub lines. This phenomenon can be attributed to the fact that at the odd-mode frequencies, the cross-section A–A' behaves like an ideal electric wall, leading to a maximum terminal current density. In contrast, during the even-mode frequency operation, the terminal current density reaches its minimum value. Figure 4 shows the change in the center frequency of the first passband (f_1) and third passband (f_3) for different H_1 and H_2 values. Figure 4(a) shows that when $H_2 = 2.2$ mm, the center frequency of the SIHRR changes with the change in H_1, and the results indicate that the change in H_1 has an impact on both f_1 and f_3. The frequency changes in the SIHRR for different H_2 values when $H_1 = 3$ mm are shown in Fig. 4(b). The change in H_2 affects f_3 but has no influence on f_1. Therefore, f_1 and f_3 could be used to adjust H_1 and H_2 independently.

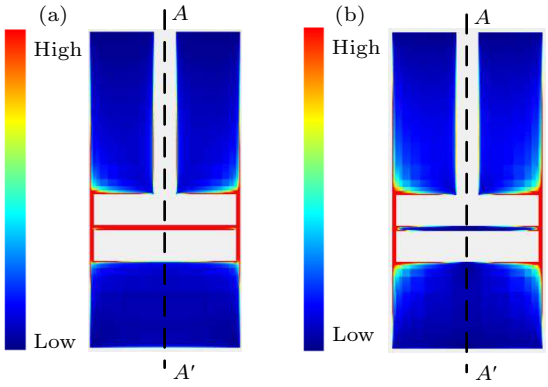


Fig. 3. Simulated current density distribution: (a) odd mode, (b) even mode.

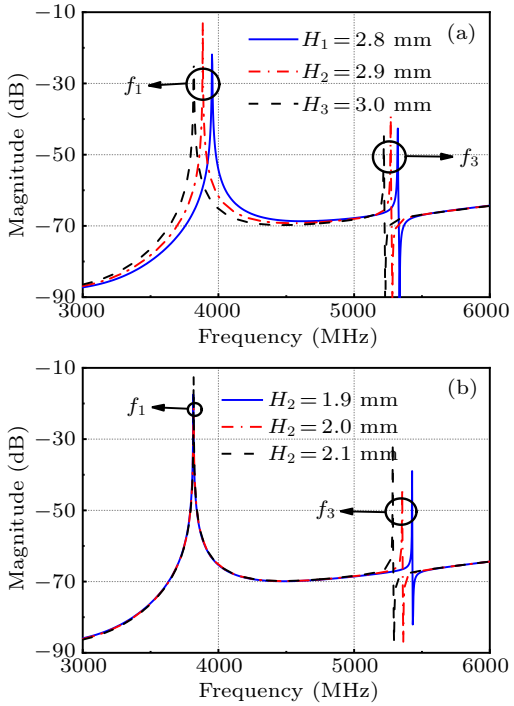


Fig. 4. (a) Effect of H_1 change on frequency, (b) effect of H_2 change on frequency.

3. Filter design

3.1. Coupling structure between resonators

The three passbands were 3430 MHz–3570 MHz, 4230 MHz–4370 MHz, and 5060 MHz–5310 MHz. Sonnet software was used to simulate the design on the MgO substrate, and the relative dielectric constant and thickness were 9.8 and 0.5 mm, respectively. For the designed third-order filter, the lumped circuit elements of the low-pass prototype filter were defined as $g_1 = 0.6291$, $g_2 = 0.9702$, $g_3 = 0.6291$,

and $g_4 = 1$. Consequently, the coupling coefficients were derived to be $M_{12}^{\mathrm{I}} = M_{23}^{\mathrm{I}} = 0.0255$, $M_{12}^{\mathrm{II}} = M_{23}^{\mathrm{II}} = 0.0267$, and $M_{12}^{\mathrm{III}} = M_{23}^{\mathrm{III}} = 0.0319$. Two distinct coupling modes can be established based on the proposed resonator structure, as illustrated in Figs. 5(a) and 5(b). These modes are classified as type-I and type-II couplings. When designing tri-band filters, it is challenging to adjust a single coupling gap to satisfy the requirements for all three passbands simultaneously. Therefore, introducing a secondary coupling structure is essential. To facilitate this design process, an appropriate initial value for the coupling distance l was selected based on the specifications of the second passband, and this value was determined to be 0.83 mm. Subsequently, an H-type secondary coupling structure was introduced to fine-tune the coupling strength of both outer passbands. The dimensions and spacing of the H-type secondary coupling structure were determined according to the required coupling strengths for the first- and third-pass bands. Through Sonnet simulation analysis, it was observed that when no secondary coupling structure was introduced, the coupling strength of type I was significantly lower than that of type II. Thus, this design adopted a type-II coupling structure.

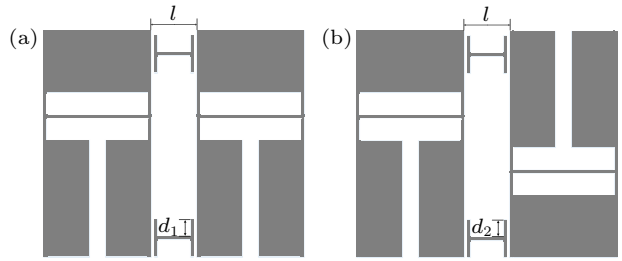


Fig. 5. Two kinds of coupling structures: (a) type I, (b) type II.

In this design, the gap between the H-type secondary coupling structure and the resonator was set to 0.1 mm; the linewidth of the secondary coupling line was set to 0.08 mm and the height to 1.12 mm.

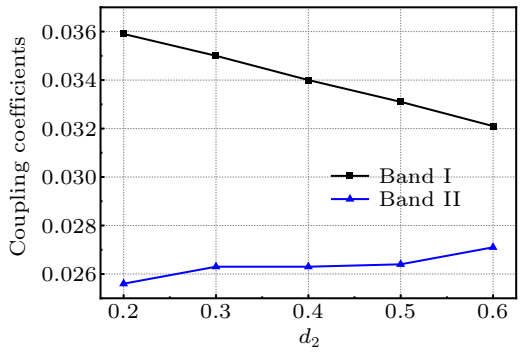


Fig. 6. Relationship between the coupling coefficient and the gap d_2.

Figure 6 illustrates the variation in coupling strength between the two resonators as a function of d_2, where l is 0.83 mm. As d_2 increased from 0.2 mm to 0.6 mm, the coupling strength of the first passband decreased significantly and showed larger variations. By contrast, the coupling strength of the third passband increased slightly; however, this change was minimal. Consequently, d_2 can be finely adjusted to achieve optimal internal coupling for both passbands.

3.2. External coupling structure

The external coupling structure illustrated in Fig. 7 was employed to obtain the external quality factors of the three passbands. This structure comprises a vertical microstrip line, a zigzag microstrip line, and an input microstrip line. The external quality factor of the filter can be derived using[15]:

$$Q_{\mathrm{e}} = \frac{f_0}{\Delta f_{3-\mathrm{dB}}}, \tag{1}$$

where f_0 and $\Delta f_{3-\mathrm{dB}}$ denote the resonant frequency and the 3 dB bandwidth of S_{21} at resonance, respectively.

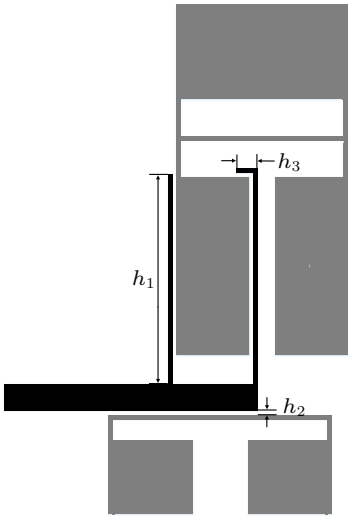


Fig. 7. External coupling structure of the resonator.

The effect of the tap position on the microstrip line on the external quality factor is shown in Fig. 8. When $h_2 = 0.07$ mm and $h_3 = 0.4$ mm, variations in Q_{e} with respect to changes in h_1 are shown in Fig. 8(a). As h_1 increased, Q_{e1} (first passband with external coupling) decreased, Q_{e2} (second passband with external coupling) increased, whereas Q_{e3} (third passband with external coupling) experienced a slight decrease. In Fig. 8(b), when $h_1 = 4.5$ mm and $h_3 = 0.4$ mm, we examine how variations in h_2 affect Q_{e}. An increase in h_2 resulted in an increase in Q_{e2}, whereas both Q_{e1} and Q_{e3} decreased slightly. Figure 8(c) illustrates how Q_{e} varies with changes in h_3, while h_1 and h_2 are maintained at constant values of 4.5 mm and 0.07 mm, respectively. As h_3 increased, all three passband external quality factors decreased.

Based on this analysis, the design process for the externally coupled structure proceeds as follows: first, integrate the value for h_3, ensuring that the desired Q_{e3} requirements are met; second, determine h_1 by selecting appropriate Q_{e1} values for the first passband according to Fig. 8(a); and finally, establish h_2 based on the expected Q_{e2} values for the second passband.

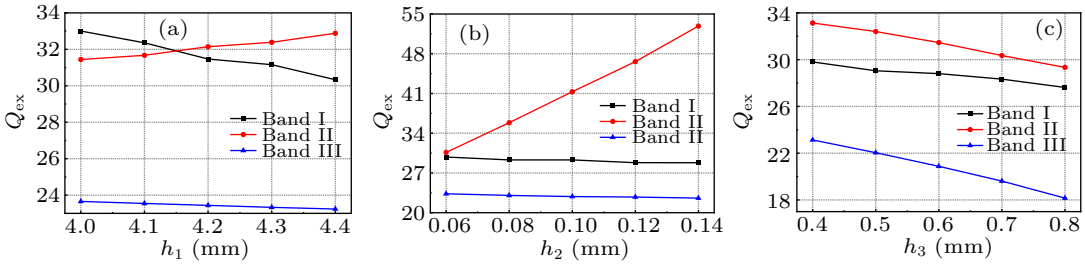


Fig. 8. Effect of microstrip tap position on external coupling: (a) h_1, (b) h_2, (c) h_3.

4. Filter fabrication and measurement

The designed third-order tri-band filter was fabricated on an MgO substrate with a double-sided YBCO film using photolithography and ion-etching techniques.[16–18] Figure 9 shows a photograph of the fabricated high-temperature superconducting (HTS) filter. The frequency response measured by the vector network analyzer at an input power of 0 dBm and a temperature of 60 K is presented in Fig. 10. The center frequencies of the three passbands were 3490 MHz, 4290 MHz, and 5190 MHz, with corresponding bandwidths of 120 MHz, 140 MHz, and 260 MHz, respectively. The in-band insertion losses of the three passbands are 0.51 dB, 0.64 dB, and 0.54 dB, respectively, and the in-band return losses were better than 27.78 dB, 18.70 dB, and 17.52 dB for each band. Additionally, Fig. 11 depicts the wide-band response of the filter; the out-of-band rejection exceeds 37 dB over a range of up to 12.6 GHz. Table 1 presents a comparison between the performance of this design and that of other tri-band filters. It can be seen from the comparison that this design has good wide stopband characteristics and lower insertion loss.

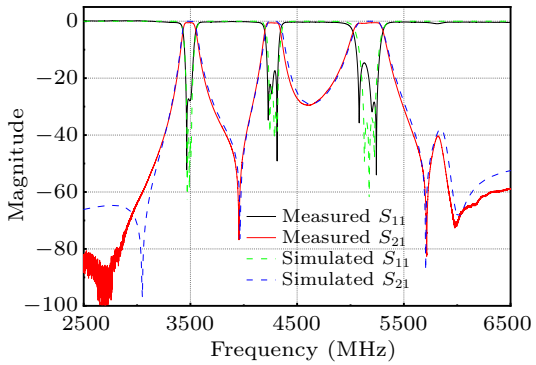


Fig. 10. Simulated and measured diagram of the tri-band HTS filter.

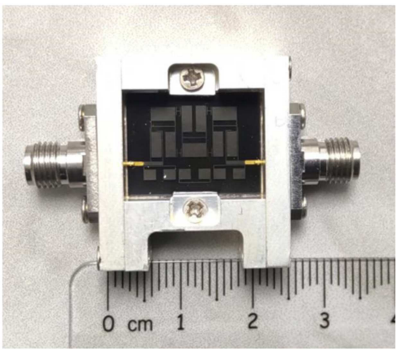


Fig. 9. Photograph of the fabricated HTS filter with connectors.

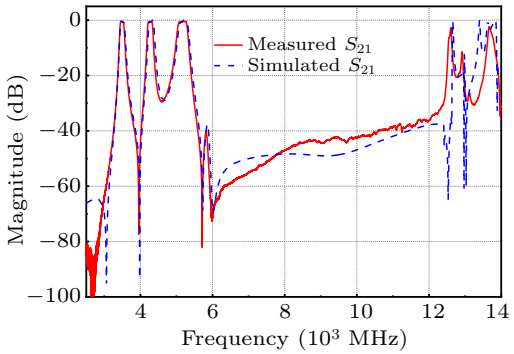


Fig. 11. Wide-band responses of the third-order filter.

Table 1. Comparisons of the proposed filter with filters designed in other works.

Reference	f_0 (GHz)	FBW (%)	Tzs	IL (dB)	RL (dB)	f_{SB1} (GHz)	size ($\lambda_g \times \lambda_g$)
[1]	1.57/3.5/5.5	12.7/10.7/9	4	0.1/0.2/0.66	25.16/26.2/28.4	–	0.18×0.15
[4]	1.51/3.49/5.79	–	5	0.1/0.12/0.16	–	–	0.066×0.051
[13]	1.502/2.003/2.498	2.1/2.1/2.3	8	0.101/0.112/0.115	–	–	0.435×0.423
[15]	1.5/2.57/3.83	–	3	2.2/1.0/1.5	11.3/11.3/11.3	> 13.7	0.12×0.14
[19]	1.575/2.4/3.5	5.2/4.25/2.7	3	0.1/0.09/0.11	–	–	0.076×0.26
This work	3.49/4.29/5.19	3.6/3.4/5.1	3	0.5/0.6/0.5	27.78/18.70/17.52	> 12.6	0.53×0.3

5. Conclusion

A tri-band frequency bandpass filter has been designed utilizing SIHRR–SIR and secondary coupling structures; this paper provides a detailed introduction to the filter's design process. The compact dimensions measure only 14 mm×18 mm, which is equal to $0.53\lambda_g \times 0.3\lambda_g$ (where λ_g is the guided wavelength of the microstrip line at the center frequency of the first

passband), and the final test results align closely with simulation outcomes — demonstrating excellent out-of-band suppression capabilities. The feasibility of this design is thus validated.

Acknowledgement

Project supported by the National Natural Science Foundation of China (Grant Nos. 61901270 and 62201464).

References

[1] Guan X H, Peng Y, Liu H W, Lei J H, Ren B P, Qin F, Wen P, Liu F and Liu Y D 2016 *IEEE Transactions on Applied Superconductivity* **26** 1501905

[2] Heng Y, Guo X B, Cao B S, Wei B, Zhang X P, Chen W, Ying Z J and Song X K 2013 *Electron. Lett.* **49** 10

[3] Akkaralaertsest T, Tubtongdee S, Sirikham A, Konpang J and Intarawiset N 2023 *RMUTL Engineering Journal* **8** 1

[4] Chu Q X, Wu X H and Chen F C 2011 *IEEE Microwave and Wireless Components Letters* **21** 655

[5] Li D T, Wang D W, Liu Y, Chen X Q and Wu H W 2019 *IEEE MTT-S International Wireless Symposium* (IWS)

[6] Liu H W, Wang Y, Wang X M, Lei J H, Xu W Y, Zhao Y L, Ren B P and Guan X H 2013 *IEEE Microwave and Wireless Components Letters* **23** 10

[7] Wu D, Wei B, Lu X L, Lu X X, Guo X B and Cao B S 2018 *Chin. Phys. B* **27** 068503

[8] Chu Q X, Wu X H and Chen F C 2011 *IEEE Microwave and Wireless Components Letters* **21** 655

[9] Zhang X Y, Xue Q and Hu B J 2010 *IEEE Microwave and Wireless Components Letters* **20** 262

[10] Wang D, Wei B, Heng Y and Cao B S 2017 *Chin. Phys. B* **26** 108502

[11] Mo Y X, Song K J and Fan Y 2014 *IEEE Microwave and Wireless Components Letters* **24** 333

[12] Song F, Wei B, Zhu L, Feng Y N, Wang R X and Cao B S 2016 *IEEE Transactions on Applied Superconductivity* **26** 8

[13] Unno T and Sekiya N 2018 *IEEE Transactions on Applied Superconductivity* **28** 1500105

[14] Hong J S and Lancaster M J 2001 *Microwave Filter for RF/Microwave Application New York: Wiley*

[15] Li C Y, Chen J X, Tang H, Zhou L H, Shi J and Bao Z H 2012 *Journal of Electromagnetic Waves and Applications* **4** 27

[16] Liu G, Li Y H, Jia B N, Gao Y P, Han L H, Lu P F and Song H Z 2023 *Chin. Phys. B* **32** 034213

[17] Xiong P Y, Chen F C, Feng Z P, Yang J T, Xia Y D, Yuan Y F, Wang X, Yuan J, Wu Y and Shi J 2023 *Chin. Phys. B* **32** 077402

[18] Sheng Z B, Chen F C, Xiong P Y, Yi Q R, Yuan J, Chen Y, Gu Y L, Jin K, Wang H H and Li X L 2025 *Chin. Phys. B* **34** 046105

[19] Liu H W, Wang Y F, Wen P and Zheng S Y 2019 *IEEE Access* **7** 32504